Article:
Arab Ansari, S., Davidson, J. and Foster, M.P. (2023) Inserted-shunt integrated planar transformer with low secondary leakage inductance for LLC resonant converters. IEEE Transactions on Industrial Electronics, 70 (3). pp. 2652-2661. ISSN: 0278-0046

https://doi.org/10.1109/TIE.2022.3165259

Inserted-shunt Integrated Planar Transformer with Low Secondary Leakage Inductance for LLC Resonant Converters

Sajad A. Ansari, Jonathan N. Davidson and Martin P. Foster

***Abstract*—The leakage inductance of an integrated transformer is usually utilised as the series inductor of an LLC topology. However, leakage inductance exists on both primary and secondary sides of an integrated transformer and secondary leakage inductance leads the control and design of the converter to difficulty. In this paper, a novel topology for inserted-shunt integrated transformers is proposed which has low secondary leakage inductance. The inserted shunt of the proposed topology is not segmental and can be located conveniently within the transformer. In addition, the inserted shunt does not require low permeability core material, simplifying its manufacture. The design and modelling of the proposed transformer topology are presented and verified by finite-element analysis and experimental implementation. The proposed topology is also compared with a recently published inserted-segmental-shunt integrated transformer. It is shown that the proposed transformer provides higher efficiency and lower AC resistance. Finally, an LLC resonant converter is implemented to examine the performance of the proposed integrated transformer in practice.**

***Index Terms*—Integrated transformer, LLC resonant converter, secondary leakage inductance.**

I. Introduction

INCREASE in power density alongside efficiency has been the trend for DC-DC power converters in recent years [1-4]. High power density can be achieved by increasing the switching frequency of the converters. However, the switching frequency must be limited in hard-switched pulse-width-modulated (PWM) converters like buck and boost converters since it causes high switching losses [5-7]. Resonant converters benefit from soft-switching capability inherently and therefore they can provide both high efficiency and power density. The LLC topology, shown in Fig. 1, is one of the most well-known resonant converters because of its unique advantages, especially its ability to repurpose the leakage and magnetising inductances of the transformer as the series and parallel inductances of the LLC tank [8-10]. Integrating magnetic components of an LLC converter into a single magnetic device enhances the power density and efficiency. Therefore, a lot of research for integrating magnetic components of LLC converters have been conducted [11].

The leakage inductance of a transformer can be used as the series inductor of the LLC tank [12-14]. However, in this approach, the leakage inductance cannot be changed for different values and is determined based on the geometry of the core and windings.

Alternatively, a structure in which the transformer has three windings—two windings for the transformer coiled around one leg and one winding coiled around another leg of cores for the series inductor—can be used [15, 16]. However, this structure suffers from higher conduction losses due to the auxiliary winding and eddy-current effect and low flexibility in design process.

A further alternative is presented in [16-20] where the core of the transformer is manipulated to integrate both inductor and transformer cores into one core and either the primary or secondary windings is merged with the winding of the series inductor. Nonetheless, in this approach, a new type of core with unusual shape that is not readily available in the market is needed for every design.

Leakage inductance can be also enhanced by interposing magnetic paper between winding layers [21]. However, the conduction losses of the winding increase in this topology due to the high eddy-current effect.

An interleaved or a semi-interleaved windings structure can provide a lower AC resistance and a controllable leakage inductance [22, 23]. Nevertheless, in these approaches, the winding structure is complicated and the leakage and magnetising inductances are not decoupled and cannot be regulated separately, making the design process more complicated. Moreover, the primary and secondary windings are coiled around the outer legs, leading to a larger footprint for

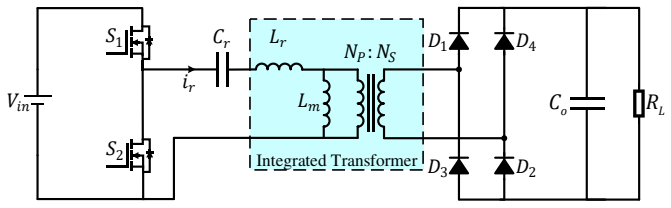

Fig. 1. Topology of the half-bridge LLC resonant converter.

S. A. Ansari, J. N. Davidson and M. P. Foster are with the Department of Electronic and Electrical Engineering, University of Sheffield, Sheffield, S1 3JD, United Kingdom (e-mail: sarabansari1 @sheffield.ac.uk; jonathan.davidson@sheffield.ac.uk; m.p.foster @sheffield.ac.uk).

This work was supported by the Engineering and Physical Sciences Research Council (EPSRC) under grant EP/S031421/1.

the transformer, lower power density and potentially higher electromagnetic interference (EMI) for the converter. Furthermore, in the interleaved winding structure, there is a high overlap area between the primary and secondary windings, which could increase the inter-winding capacitance to an undesirable value.

A low-permeability magnetic shunt, such as a powder core, can be inserted into a planar transformer to achieve a high leakage inductance while the leakage and magnetising inductance are decoupled from each other and the readily available planar cores in the market can be used without any manipulation [24-26]. In this topology, which is known as inserted-shunt integrated transformer, there is no need for either an auxiliary winding or an unusual magnetic core and all three magnetic components of the isolated LLC converter can be integrated into only a single planar transformer. This topology also benefits from the advantages of planar transformers, viz high power density, improved cooling capability, modularity and manufacturing simplicity. However, the inserted shunt must have a specific and unusually low permeability in this topology, leading the design and manufacturing to difficulty and higher cost. Therefore, two new topologies are suggested in [27, 28] to address this problem. The magnetic shunt in these structures is formed by interleaving high permeability ferrite with thin plastic spacers to form a distributed air gap ferrite shunt with the same bulk permeability as the conventional low-permeability shunt. The design becomes more economical in these structures because high-permeability materials like ferrite, which is widely available in different sizes and for lower price, can be used for the shunt. However, in these structures, the inserted shunt has several segments and must be placed in between two E-cores which makes the implementation difficult. In addition, in all of the structures with an inserted shunt [24-29], the main issue is that the leakage inductance does not only increase in the primary side but also it increases in the secondary side.

The effects of secondary leakage inductance on LLC resonant converters are investigated in [30]. First-harmonic approximation (FHA) has been usually used to analyse the LLC topology while the secondary leakage inductance is ignored. However, the voltage gain of an LLC converter is very sensitive to resonant components and ignoring the secondary leakage inductance causes inaccurate analysis [19, 31]. Alternatively, the primary and secondary leakage inductances are considered identical in many studies and the secondary leakage inductance is referred to the primary side of the simplified equivalent circuit according to transformer turns ratio. However, this method is also not precise, especially when the magnetising inductance is purposefully reduced by inserting air gaps in transformer cores [32]. Some research have been done to model the LLC converter while the secondary leakage inductance is considered [31, 33]. Even though these models estimate the gain of the converter more precisely, the design of the converter and its control system is more complicated when there is a high secondary leakage inductance [34] and thus it is still preferred to have a negligible leakage inductance on the secondary side.

Zhang, *et al*, [35] point out that, in LLC resonant converters for voltage regulator modules (VRM), the synchronous rectifier switches employ a self-driven method. In this situation, when the leakage inductance exists on the secondary side, there is an overlapping period of commutation between the secondary switches and their currents, leading to higher losses. In addition, Noah, *et al*, [32] found that the secondary leakage inductance causes some other major problems. Firstly, the secondary leakage inductance adds a virtual gain to the gain curve of the LLC converter and the converter encounters a non-unity gain at the nominal frequency, leading the control system to difficulty. Secondly, it limits the current delivered to the load by increasing the converter output impedance.

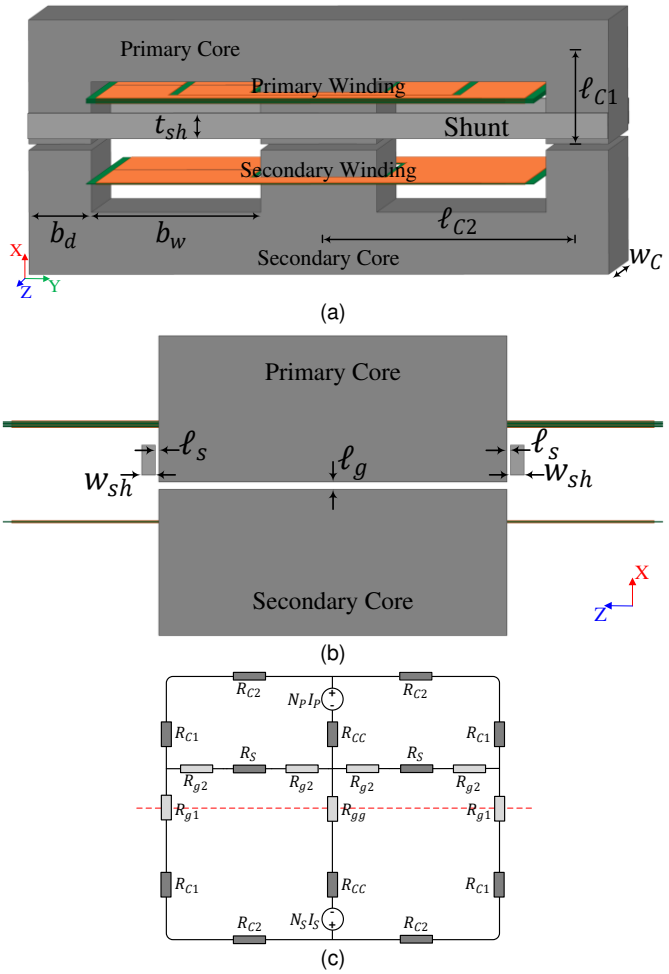

Fig. 2. The proposed integrated transformer. (a) Schematic in x-y plane. (b) Schematic in x-z plane. (c) Reluctance model.

It should be pointed out that the integrated transformers can also be used in other similar topologies like phase-shifted full-bridge converters. Therefore, it is preferred that the leakage inductance only increases on one side and the topology of the converter remains the same as the original topology to avoid unnecessary new analysis and modification for each type of converter.

In this paper, a new structure for the inserted-shunt integrated transformers is proposed to address the key issue of reducing high secondary leakage inductance. Fig. 2 shows the structure and reluctance model of the proposed integrated magnetic transformer. Fig. 2(a) shows the transformer in the x-y plane

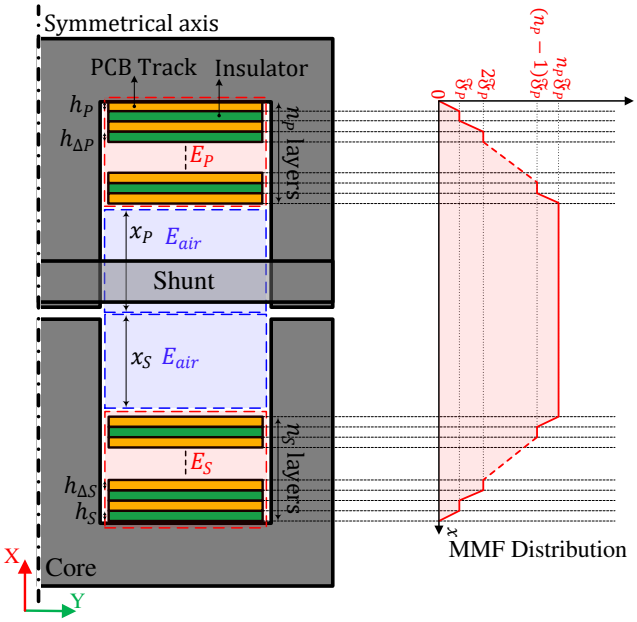

Fig. 3. MMF distribution for the proposed integrated transformer.

and is divided into a primary section (consisting of an E-core half and winding) and a secondary section separated by an air gap. Two shunts are placed across x-y faces of the primary E-core. Fig. 2(b) shows the location of the shunts in the x-z plane. Since the shunts only provide a low-reluctance route for leakage flux of the primary winding, the primary leakage inductance only increases. In the proposed structure, the bulk permeability of the shunts can be regulated by changing their distances from the core rather than changing the air gaps length across them, which is in contrast with the segmental-shunt topology presented in [27, 28]. Hence, the proposed structure not only has the advantage of using high-permeability materials for the shunts but also requires solid, rather than segmental shunts.

The proposed structure is analysed and modelled in detail. The theoretical analysis is verified by finite-element analysis (FEA) simulation and experimental results. An efficiency comparison and AC resistance analysis for the proposed structure and a recent structure with inserted-segmental-shunt presented in [27, 28] are provided. In addition, the performance of the proposed integrated transformer is investigated in practice by implementing an isolated LLC resonant converter. The experimental results show that the proposed structure can integrate all three magnetic components of an LLC converter into a single planar transformer.

The paper is organised as follows: the proposed integrated transformer with low secondary leakage inductance is modelled in Section II. In Section III, theoretical analysis is verified by a simulation study. In Section IV, experimental verification of the proposed modelling and integration capability of the proposed structure are presented. The conclusion of the work is finally provided in Section V.

II. Proposed Integrated Magnetic Transformers

The schematic of the proposed structure, geometry/dimensions and reluctance model are shown in Figs. 2(a), (b) and (c), respectively. An air gap ℓ_g is inserted between the E-cores to regulate magnetising inductance and an air gap ℓ_s is located in between shunts and primary E-core to adjust the leakage inductance. The dashed line shown in the reluctance model, Fig. 2(c), divides the contribution into primary section (above the line) and secondary section (below the line) with the dividing line crossing air gap reluctances $\mathcal{R}_{g1}$ and $\mathcal{R}_{gg}$. The flux produced by the magnetic field of the current in the primary winding that links with the secondary winding is reduced by the reluctance route provided by the inserted shunts. However, this route does not affect the flux produced by the magnetic field of the current in the secondary winding that links with the primary winding since core reluctances, $\mathcal{R}_{C1}$, $\mathcal{R}_{C2}$ and $\mathcal{R}_{CC}$ are negligible compared to air gap reluctance of the shunt, $\mathcal{R}_{g2}$.

In the following this section, the modelling of the proposed structure is discussed for estimation of the leakage and magnetising inductances.

Assuming the permeability of the core is very high then any energy that is stored in the transformer must be located outside of the core. Equation (1) shows the energy stored in the volume of the winding, window area and shunt is equal the energy stored in the leakage inductance, L_{lk}.

$$E = \frac{1}{2}\iiint_V BH \,\mathrm{d}V = \frac{1}{2}L_{\mathrm{lk}}I_{\mathrm{P}}^2 \tag{1}$$

where V is the total volume of window area, windings and inserted-shunts, I_{P} is the RMS of primary current, B is the flux density and H is the magnetic field intensity.

The energy stored in the winding window area of cores and primary and secondary windings alongside the inserted shunts form the total energy stored by the leakage inductance. Fig. 3 shows a cross-section of the right hand side of the transformer divided into several regions contributing the stored leakage energy. The primary winding consists of N_{P} turns and is constructed from n_{P} layers each with k_{P} turns ($N_{\mathrm{P}} = k_{\mathrm{P}}n_{\mathrm{P}}$). Each primary winding layer has a height h_{P} and an associated insulating layer with a height $h_{\Delta\mathrm{P}}$. Similar notation is used for the secondary winding, $N_{\mathrm{S}} = k_{\mathrm{S}}n_{\mathrm{S}}$, with each layer having a height h_{S} and insulating layer height $h_{\Delta\mathrm{S}}$. Regions E_{P} and E_{S} refer to the energy stored in the primary and secondary winding. E_{air} is the energy stored proportion of the winding window not occupied by the windings and this is divided into a primary region of height x_{P} and a secondary region of height x_{S}. Therefore, the energy stored in each part needs to be obtained first and the total leakage inductance can be then calculated by their summation and (1).

A. Energy stored in window area – E_{air}.

The magnetomotive force (MMF) of each layer of the primary winding, $\mathfrak{F}_{\mathrm{P}}$, may be obtained from (2), where k_{P} is the number of turns in each layer of the primary winding.

$$\mathfrak{F}_{\mathrm{P}} = k_{\mathrm{P}}I_{\mathrm{P}} \tag{2}$$

If n_{P} and n_{S} are defined as the number of layers of the primary and secondary windings, respectively, the MMF within the window area, $\mathfrak{F}_{\mathrm{air}}$, is equal to $n_{\mathrm{P}}\mathfrak{F}_{\mathrm{P}}$ and the magnetic field intensity within the air area, H_{air}, may be obtained by (3).

$$H_{\text{air}} = \frac{n_{\text{P}}\Im_{\text{P}}}{b_w} \tag{3}$$

From (1), the stored energy in not winding occupied region, E_{air}, (defined in Fig. 3) can be obtained as (4).

$$E_{\text{air}} = \frac{1}{2}\mu_0 w_c b_w \int_{-x_{\text{S}}}^{x_{\text{P}}} H_{air}^2 \mathrm{d}x \tag{4}$$

where w_c is the core depth and x_{P} and x_{S} are the distances from the primary and secondary windings to the centre of the transformer, respectively, defined in Fig. 3. From (2)-(4), E_{air} in both windows (left and right windows of an E core) can be obtained as follows:-

$$E_{\text{air}} = \mu_0 w_c \frac{n_{\text{P}}^2 k_{\text{P}}^2 I_{\text{P}}^2}{b_w}(x_{\text{P}} + x_{\text{S}}) \tag{5}$$

B. Energy stored in primary and secondary PCB windings

From the MMF distribution presented in Fig. 3 which has been obtained based on method outlined in [14, 24, 25], the stored energy in PCB layers of primary and secondary windings can be obtained. Ouyang, et al, [14] proved that energy stored in the primary and secondary windings may be calculated as (6) and (7), respectively.

$$E_{\text{P}} = \frac{1}{6}\mu_0 \frac{w_c}{b_w} k_{\text{P}}^2 [h_{\Delta\text{P}}(2n_{\text{P}}^3 - 3n_{\text{P}}^2 + n_{\text{P}}) + 2h_{\text{P}} n_{\text{P}}^3] I_{\text{P}}^2 \tag{6}$$

$$E_{\text{S}} = \frac{1}{6}\mu_0 \frac{w_c}{b_w} k_{\text{S}}^2 [h_{\Delta\text{S}}(2n_{\text{S}}^3 - 3n_{\text{S}}^2 + n_{\text{S}}) + 2h_{\text{S}} n_{\text{S}}^3] I_{\text{S}}^2 \tag{7}$$

In (6) and (7), h_{P} and h_{S} are defined as the thickness of the PCB tracks of the primary and secondary windings, respectively, and $h_{\Delta\text{P}}$ and $h_{\Delta\text{S}}$ are defined as the thickness of the PCB insulation layers of the primary and secondary windings, respectively.

C. Energy stored in inserted shunts

The stored energy in the inserted shunts can be obtained from the reluctance model using the method outlined by Ansari, *et al*, [27, 28]. Referring to Fig. 2(c), $\mathcal{R}_{\text{g1}}$, $\mathcal{R}_{\text{gg}}$ and $\mathcal{R}_{\text{g2}}$ are air gap reluctances, $\mathcal{R}_{C1}$, $\mathcal{R}_{C2}$ and $\mathcal{R}_{CC}$ are core reluctances and $\mathcal{R}_{\text{S}}$ is shunt reluctance and they can be calculated by (8)-(14). In the provided reluctance modelling, it is assumed that both shunts are located at the same distance from the cores (ℓ_{s}), and therefore only a single shunt of double thickness ($2t_{\text{sh}}$) needs to be considered.

$$\mathcal{R}_{C1} = \frac{\ell_{C1}}{\mu_0 \mu_r b_d w_c} \tag{8}$$

$$\mathcal{R}_{C2} = \frac{\ell_{C2}}{\mu_0 \mu_r b_d w_c} \tag{9}$$

$$\mathcal{R}_{CC} = \frac{\ell_{C1}}{\mu_0 \mu_r A_c} \tag{10}$$

$$\mathcal{R}_{\text{S}} = \frac{b_w}{2\mu_0 \mu_s t_{\text{sh}} w_{\text{sh}}} \tag{11}$$

$$\mathcal{R}_{\text{g1}} = \frac{\ell_{\text{g}}}{\mu_0 (b_d + \ell_{\text{g}})(w_c + \ell_{\text{g}})} \tag{12}$$

$$\mathcal{R}_{\text{g2}} = \frac{\ell_{\text{s}}}{2\mu_0 (b_d + \ell_{\text{s}})(t_{\text{sh}} + \ell_{\text{s}})} \tag{13}$$

$$\mathcal{R}_{\text{gg}} = \frac{\ell_{\text{g}}}{\mu_0 (2b_d + \ell_{\text{g}})(w_c + \ell_{\text{g}})} \tag{14}$$

where μ_0, μ_r and μ_s are the permeability of the air, and the relative permeability of the core and shunt, respectively. A_{C} is the core effective cross-sectional area and other variables are defined in Fig. 2(a). Hurley, *et al*, [36] showed that an effective cross-sectional area of the air gap with dimension *a* by *b* are equal to (*a*+*g*) by (*b*+*g*) when the fringing effect is considered and *g* is the length of the studied air gap.

From the reluctance model presented in Fig. 2(c) and the method outlined by Ansari et al [27, 28], the magnetising inductance of the proposed integrated transformer (evaluated at the primary side) can be obtained as follows:-

$$L_{\text{m}_\text{P}} = \frac{2N_{\text{P}}^2}{\mathcal{R}_A \mathcal{R}_B - (2\mathcal{R}_{\text{g2}} + \mathcal{R}_{\text{S}})} \tag{15}$$

where $\mathcal{R}_A$ and $\mathcal{R}_B$ can be defined as (16) and (17), respectively.

$$\mathcal{R}_A = \frac{\mathcal{R}_{\text{g1}} + 2\mathcal{R}_{\text{gg}} + \mathcal{R}_B}{2\mathcal{R}_{\text{g2}} + \mathcal{R}_{\text{S}}} \tag{16}$$

$$\mathcal{R}_B = \mathcal{R}_{C1} + \mathcal{R}_{C2} + 2\mathcal{R}_{CC} + 2\mathcal{R}_{\text{g2}} + \mathcal{R}_{\text{S}} \tag{17}$$

And the primary self-inductance can be obtained by

$$L_{\text{PP}} = \frac{N_{\text{P}}^2}{\mathcal{R}_{T_P}} \tag{18}$$

where $\mathcal{R}_{T_P}$ is the core reluctance (evaluated from the primary side) and can be obtained as (19).

$$\mathcal{R}_{T_P} = \mathcal{R}_{CC} + \frac{\mathcal{R}_{C1} + \mathcal{R}_{C2}}{2} + \frac{(2\mathcal{R}_{\text{gg}} + 2\mathcal{R}_{CC} + \mathcal{R}_{\text{g1}} + \mathcal{R}_{C1} + \mathcal{R}_{C2})(2\mathcal{R}_{\text{g2}} + \mathcal{R}_{\text{S}})}{2(\mathcal{R}_{\text{g1}} + 2\mathcal{R}_{\text{gg}} + \mathcal{R}_B)} \tag{19}$$

Finally, the primary leakage inductance due to the inserted shunts, $L_{\text{lk}_\text{P}(\text{shunt})}$, can be calculated by (20) [27, 28].

$$L_{\text{lk}_\text{P}(\text{shunt})} = L_{\text{PP}} - L_{\text{m}_\text{P}} \tag{20}$$

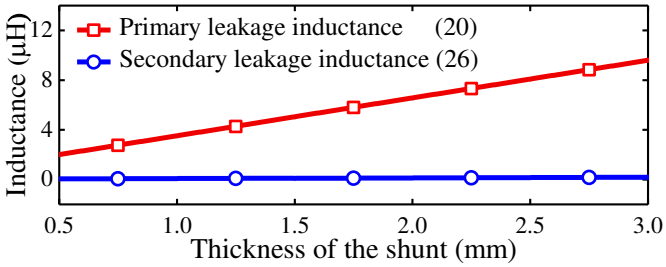

Fig. 4. Primary and secondary leakage inductances caused by the shunts. Core: E32/6/20/R-3F4, shunt material: Fair-Rite M6, ℓ_g=ℓ_s=0.3mm, w_{sh}=0.8mm, N_P=N_S=10.

The secondary magnetising inductance (using a similar approach) can be obtained as (21).

$$L_{m_S} = \frac{2N_S^2}{\mathcal{R}_C\mathcal{R}_D - (2\mathcal{R}_{g2}+\mathcal{R}_S)} \tag{21}$$

where $\mathcal{R}_C$ and $\mathcal{R}_D$ can be defined as (22) and (23), respectively.

$$\mathcal{R}_C = \frac{\mathcal{R}_B}{2\mathcal{R}_{g2}+\mathcal{R}_S} \tag{22}$$

$$\mathcal{R}_D = \mathcal{R}_{g1} + 2\mathcal{R}_{gg} + \mathcal{R}_B \tag{23}$$

And the secondary self-inductance can be obtained by

$$L_{SS} = \frac{N_S^2}{\mathcal{R}_{T_S}} \tag{24}$$

where $\mathcal{R}_{T_S}$ is the core reluctance (evaluated from the secondary side) and can be obtained as (25).

$$\mathcal{R}_{T_S} = \mathcal{R}_{gg} + \mathcal{R}_{CC} + \frac{\mathcal{R}_{g1} + \mathcal{R}_{C1} + \mathcal{R}_{C2}}{2} + \frac{(2\mathcal{R}_{CC} + \mathcal{R}_{C1} + \mathcal{R}_{C2})(2\mathcal{R}_{g2}+\mathcal{R}_S)}{2\mathcal{R}_B} \tag{25}$$

Finally, the secondary leakage inductance due to the inserted shunts, $L_{lk_S(shunt)}$, can be calculated by (26) [27, 28].

$$L_{lk_S(shunt)} = L_{SS} - L_{m_S} \tag{26}$$

In Fig. 4, from (20) and (26), the primary and secondary leakage inductances caused by shunts of different thickness are presented. As shown, the shunts do not have a noticeable influence on the secondary leakage inductance, but the primary leakage inductance can be increased by the shunts. This is because the mutual inductance from primary to secondary is reduced by the reluctance route through the inserted shunts. However, this route does not affect the flux produced by the secondary winding that links with the primary winding since core reluctances, $\mathcal{R}_{C1}$, $\mathcal{R}_{C2}$ and $\mathcal{R}_{CC}$ are negligible compared to air gap reluctance of the shunt, $\mathcal{R}_{g2}$.

As presented in Fig. 4, the secondary leakage inductance caused by the shunts can be neglected and, therefore, from (1), (5)-(7) and (20), the total leakage inductance of the proposed integrated transformer can be calculated as follows:-

$$L_{lk} = L_{lk_P(shunt)} + 2\mu_0 w_c \frac{N_P^2}{b_w}(x_P + x_S) + \frac{1}{3}\mu_0 \frac{w_c}{b_w} k_P^2 n_P^2 \sum_{i=P,S}\left[h_{\Delta i}\left(2n_i - 3 + \frac{1}{n_i}\right) + 2h_i n_i\right] \tag{27}$$

where N_P is the primary turns number. Therefore, from (15) and (27), an integrated transformer for the required magnetising and leakage inductances can be designed. For the remainder of the paper, the magnetising inductance of the transformer, L_m, is defined equal to L_{m_p}.

The calculated leakage and magnetising inductances of the proposed integrated transformer for different thicknesses of the shunt, t_{sh}, air gap length, ℓ_g, and distance between shunts and cores, ℓ_s, are presented in Figs. 5(a) and (b), using a E32/6/20/R-3F4 core as reference to determine the main factors of influence in a design (details of the geometry provided in the figure caption). It is clear that the magnetising inductance is mainly influenced by air gap length, ℓ_g, between cores and cannot be changed appreciably by varying t_{sh} and ℓ_s. However, the leakage inductance can be regulated by changing ℓ_s and t_{sh} and is not affected by ℓ_g. Therefore, in the proposed integrated transformer, the leakage and magnetising inductances are sufficiently decoupled from each other and can be separately realised, leading the design process to higher flexibility.

The modelling of the proposed integrated transformer is now fully investigated and it is shown that the transformer can be designed for most reasonable specifications in terms of leakage and magnetising inductances. These designs do not require low-permeability materials or segmental shunts and with the advantage of not increasing the leakage inductance on the secondary side. Therefore, the proposed transformer is an attractive candidate for use in an LLC resonant converter to integrate its magnetic components into a single transformer. In the following, the operation of the proposed transformer when it is designed to be used in an exemplar LLC resonant converter is investigated and its modelling is verified by FEA simulation and experimental implementation.

III. Simulation Results

An integrated transformer with minimum secondary leakage inductance is designed based on the equations provided in Section II and its specifications are presented in Table I. The magnetising and leakage inductances and turns ratio of the designed transformer are chosen according to the specification of an exemplar isolated LLC resonant converter presented in Table III. The tranformer core (E32/6/20/R-3F4) is selected based on the design guidlines outlined by the catalogue of the core provided by its manufacturer [37], which presents guidlines for appropriate core selection based on the operating frequency and power. The thickness of the shunt and air-gap

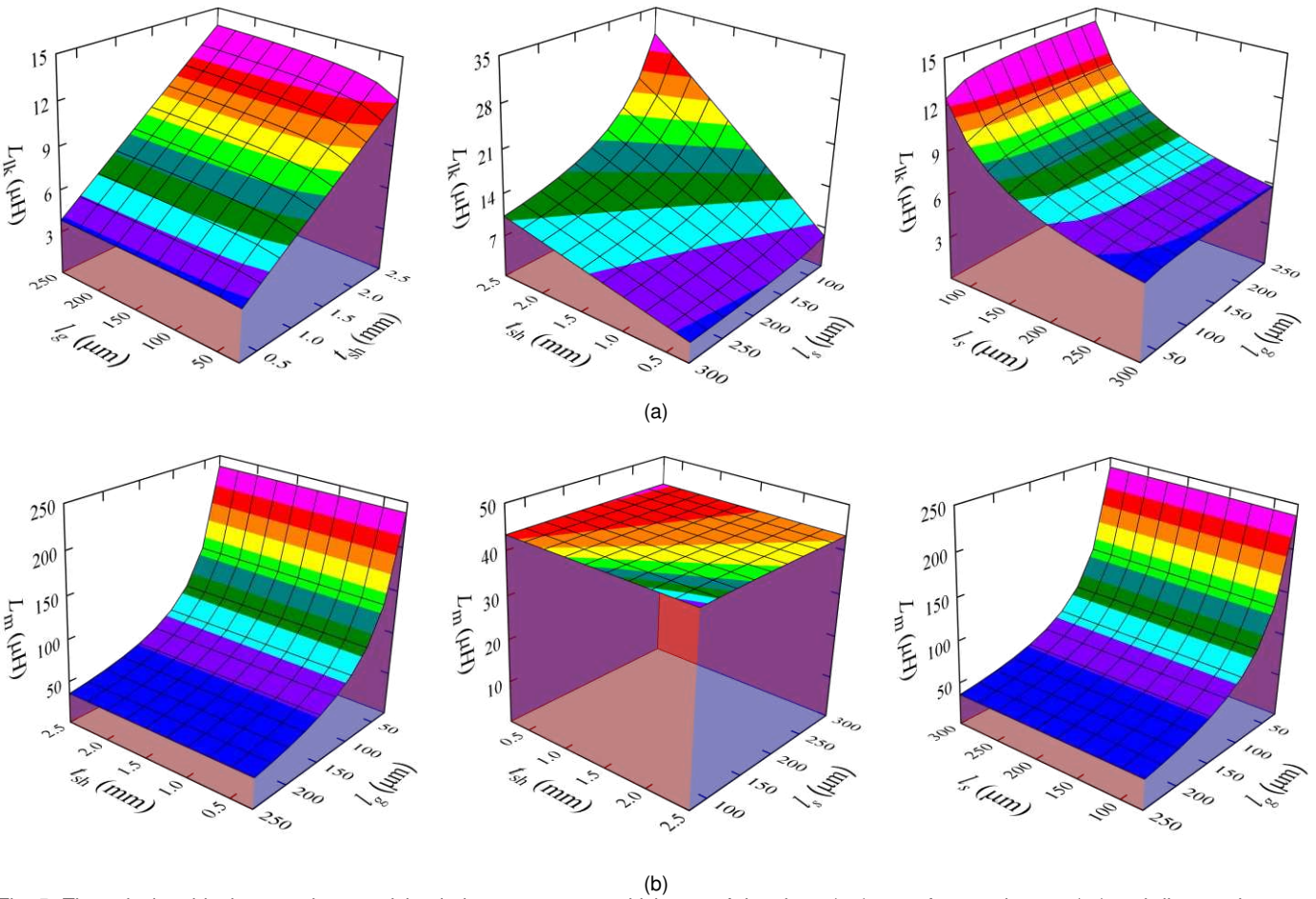

Fig. 5. The calculated leakage and magnetising inductances versus thickness of the shunt (t_{sh}), transformer air gaps (ℓ_g) and distance between shunts and cores (ℓ_s). (a) Leakage inductance. (b) Magnetising inductance. Core: E32/6/20/R-3F4, shunt material: Fair-Rite M6, t_{sh}=1mm, ℓ_g=ℓ_s=0.2mm, w_{sh}=0.8mm, N_P=10, N_S=2, n_P=5, n_S=2, k_P=2, k_S=1, x_P=2.5mm, x_S=1.5mm.

lengths (ℓ_g and ℓ_s) are estimated in order to provide the required leakage and magnetising inductances, using (15) and (27), and considering the dimensions of the selected core. Moreover, the windings are designed considering the dimensions, skin effect, their root-mean-square (RMS) currents and the difficulty of manufacturing.

To verify the theoretical analysis, the FEA simulation results of the designed tranformer are presented below.

TABLE I
PROPOSED STRUCTURE'S SPECIFICATION

Symbol	Parameter	value
N_P	Primary turns	10
N_S	Secondary turns	2
k_P	Turns per layer in primary	2
k_S	Turns per layer in secondary	1
n_P	Number of primary layers	5
n_S	Number of secondary layers	2
h_P, h_S	Primary and secondary conduction thickness	35 μm
$h_{\Delta P}$, $h_{\Delta S}$	Primary and secondary insulation thickness	30 μm
t_{sh}	Shunt thickness	1.3 mm
w_{sh}	Shunt wideness	0.8 mm
ℓ_g	Transformer air gap	0.32 mm
ℓ_s	Distance between shunt and cores	0.20 mm
x_P, x_S	Distance between primary and secondary windings and centre of E-cores, respectively	2.5 mm 1.5 mm

The magnetic field intensity and flux density vectors for the proposed topology, while it is used in an LLC converter with specification presented in Table III, are shown in Figs. 6(a) and (b), respectively. According to Fig. 6, the magnetic field intensity and flux density vectors are dominant in the shunts and their air gaps (ℓ_s) rather than windows area and PCB windings. The leakage inductance is therefore mainly caused by the inserted shunts. In addition, since the magnetic field intensity is highest in the cores air gap (ℓ_g), the magnetising inductance is mainly affected by ℓ_g.

From Fig. 6, it can be observed that the magnetic flux density for the shunts is around 0.2 T, which is below saturation. A

TABLE II
PARAMETERS OF THE IMPLEMENTED INTEGRATED TRANSFORMER

Parameter	FEA modelling	Simulation	Measurement
Magnetising inductance, L_m	28.5 μH	28.85 μH	29.5 μH
Primary leakage inductance, L_{lk_P}	8 μH	8.2 μH	8.3 μH
Secondary leakage inductance, L_{lk_S}	0.03 μH	0.04 μH	0.03 μH

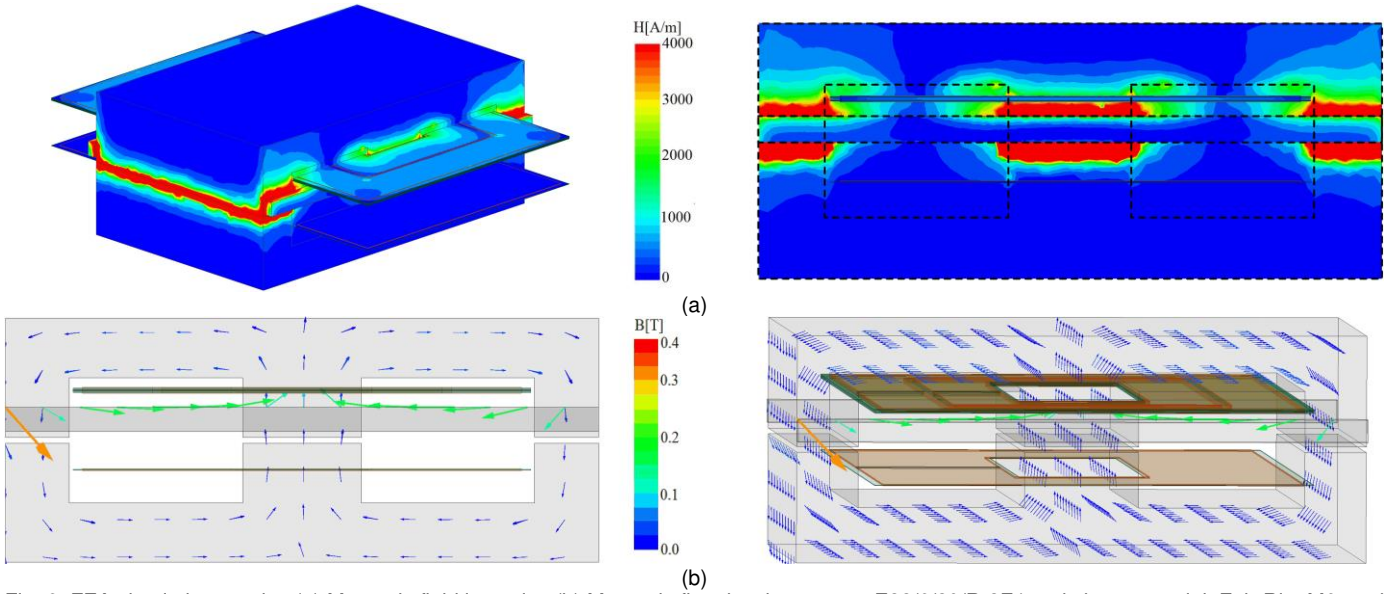

Fig. 6. FEA simulation results. (a) Magnetic field intensity. (b) Magnetic flux density vectors. E32/6/20/R-3F4 and shunt material: Fair-Rite M6, and frequency=200 kHz.

design can avoid saturation for the shunts whether a low-permeability material or high-permeability material is used for the shunts.

The leakage and magnetising inductances versus thickness of the shunt (t_{sh}) and transformer air gap (ℓ_g) obtained from (15) and (27) and measured by FEA simulation are presented for the proposed topology in Fig. 7(a) and (b), respectively. According to Fig. 7, there is a good agreement between the theoretical and simulation results, verifying the provided modelling of the proposed structure.

Primary and secondary leakage inductances caused by the shunts for the proposed integrated transformer are presented in Fig. 8. As shown, the secondary leakage inductance is not affected by the shunts' characteristics and has a negligible value, verifying Fig. 4.

Loss distribution of the proposed topology, while it is used in an LLC converter with specification presented in Table III, is presented in Fig. 9. For comparison, an integrated transformer with inserted-segmental shunt, presented in [27, 28], is also designed to the same specification and simulated, shown in Fig. 9. As shown, the proposed transformer has lower conduction losses and therefore provides higher efficiency compared to the inserted-segmental-shunt (conventional) topology.

IV. Experimental Verification

To verify theoretical analysis and simulation results, an integrated transformer based on the proposed structure with specifications presented in Table I is built and its prototype is shown in Fig. 10(a). For comparison, an integrated transformer with inserted-segmental-shunt presented in [27, 28] is also built to the same specification, shown in Fig. 10(b). The shunts for this work was made by cutting ferrite sheets and gluing them in parallel.

The measured leakage and magnetising inductances of the proposed topology at 200 kHz obtained using an Omicron Bode 100 frequency analyser are shown in Table II. According to Table II, the leakage and magnetising inductances obtained by FEA simulation and modelling are close to the experimental results. The proposed topology does not increase the secondary leakage inductance despite the inserted magnetic shunt. The secondary leakage inductance, while low, is non-zero because there is leakage flux in the window area of the E-core.

TABLE III
The Implemented LLC Converter's Specification

Symbol	Parameter	value
$N_P: N_S$	Turns ratio	10:2
L_m	Magnetising inductance	29 μH
L_r	Resonant (series) inductance	9 μH
C_r	Resonant capacitance	39 nF
V_{in}	Input voltage	45-55 V
V_{out}	Output voltage	5 V
P_{out}	Output power	25 W
f_s	Switching frequency	200-350 kHz
S	Switches	IRF530N
D	Rectifier diodes	12CTQ045

AC resistance, primary self-inductance and leakage inductance versus frequency for the proposed topology and integrated transformer with inserted-segmental-shunt (conventional) are presented in Fig. 11. As shown, the magnetising and leakage inductances of both implemented topologies are very similar. However, the integrated transformer with inserted-segmental-shunt suffers from higher AC resistance compared to the proposed topology and this is because of higher fringing fields due to the inserted-segmental-shunt topology (as already pointed in [27, 28]). Therefore, the proposed topology benefits from lower conduction losses, which verifies Fig. 9. As shown in Fig. 2, in the proposed topology, the right and left air-gaps of the shunt (labelled ℓ_s) are further from the windings, reducing their coupling with the fringing field. However, in the segmental topology (presented

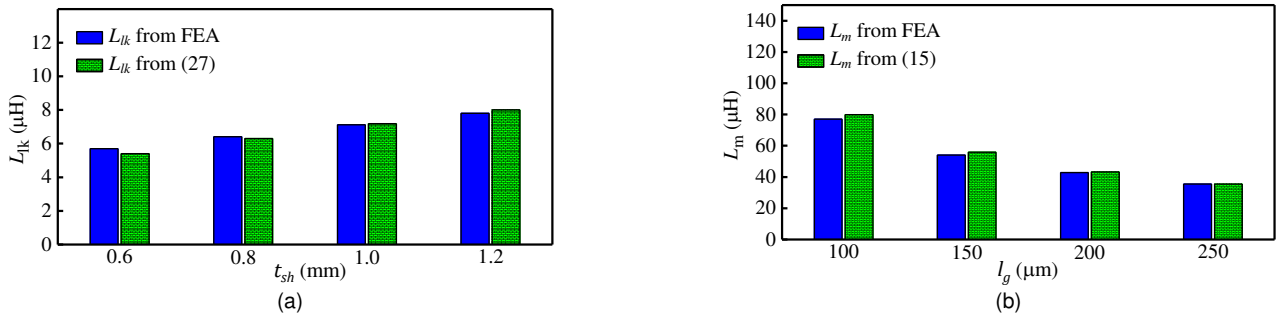

Fig. 7. Modelling validation by simulation study. (a) Leakage inductance ($l_g = 0.05mm$). (b) Magnetising inductance ($t_{sh} = 1mm$). E32/6/20/R-3F4, shunt material: Fair-Rite M6, $l_s = 0.2mm$, and frequency=200 kHz.

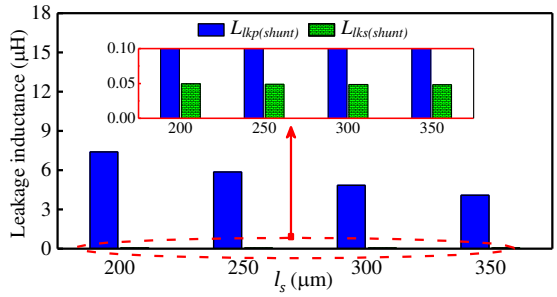

Fig. 8. Primary and secondary leakage inductances caused by the shunts. E32/6/20/R-3F4, shunt material: Fair-Rite M6, and frequency=200 kHz.

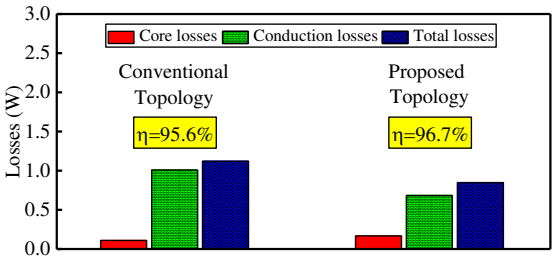

Fig. 9. Loss distribution of the proposed and conventional topologies for output power of 25W. E32/6/20/R-3F4, shunt material: Fair-Rite M6, and frequency=200 kHz.

in [27, 28]), all of the air-gaps are between the lower and upper windings and therefore they have greater coupling with the fringing field, leading to higher AC losses.

To verify the performance of the proposed integrated transformer, it was incorporated within an LLC converter designed according to the procedure outlined in [38], shown in Fig. 12. The specification of the designed LLC converter is presented in Table III in which the series and parallel inductances are integrated into the transformer. The waveforms of the LLC converter operating at 210 kHz and 280 kHz switching frequency using the proposed topology and the topology with inserted-segmental shunt are measured and presented in Figs. 13(a)-(d). It can be seen that the converter operates correctly and the MOSFETs are turned on at zero voltage switching (ZVS) because the switch gate turns on after its drain-source voltage drops to zero.

The efficiency of the LLC converter versus different loads for the proposed integrated transformer and inserted-segmental-shunt integrated (conventional) transformer is presented in Fig. 14. According to Figs. 11 and 14, the proposed topology benefits from higher efficiency compared to the topology with inserted-segmental-shunt and the lower AC resistance of the proposed topology explains the reason of this discrepancy. It needs to be pointed that the rectifier diodes cause the dominant losses in the implemented converter and it is hard to show the efficiency difference between the proposed topology and inserted-segmental-shunt integrated transformer when they are operating in the circuit. Hence, the rectifier diodes are removed from the converter to measure the efficiency.

The thermal images of the proposed integrated transformer and inserted-segmental-shunt integrated transformer while they are used in the implemented LLC resonant converter at nominal operating condition are shown in Fig. 15(a) and (b), respectively. As shown, the proposed topology operates at a lower temperature since it has lower losses, verifying Fig. 14. In addition, the temperature of windings is higher than the cores since conduction losses are the dominant losses in the inserted-shunt integrated transformers, verifying the loss distribution presented in Fig. 9.

It should be noted that the application of the proposed integrated transformer can be also extended to other similar converters like phase-shifted full-bridge converters and is not only restricted to the LLC resonant converter.

V. Conclusion

A new topology for the inserted-shunt integrated planar transformers was proposed which has low secondary leakage inductance. The proposed topology overcomes the main issue of inserted-shunt integrated transformers which is high leakage inductance in the secondary side. In addition, the proposed topology benefits from both advantages of high-permeability segmental shunt and low-permeability one-segment shunt topologies. The proposed topology is analysed and modelled in detail. It is shown that the design of leakage and magnetising inductances are decoupled from each other completely. Therefore, they can be determined separately, leading the design process to higher flexibility. FEA simulation and experimental results are presented to verify the theoretical analysis. A recently published inserted-segmental-shunt integrated transformer was compared experimentally with the proposed transformer in terms of efficiency and AC resistance and the new design is found to provide higher efficiency. In addition, an LLC resonant converter was built to investigate the performance of the proposed topology in practice. Results show that the proposed topology can integrate all three magnetic

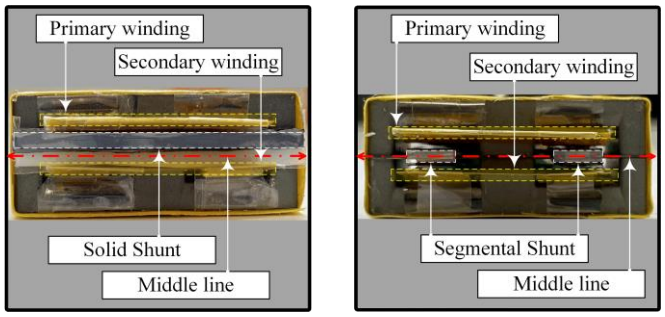

Fig. 10. Prototypes of the implemented transformers. (a) The proposed transformer. (b) The inserted-segmental-shunt transformer. Core: E32/6/20/R-3F4 and shunt material: Fair-Rite M6.

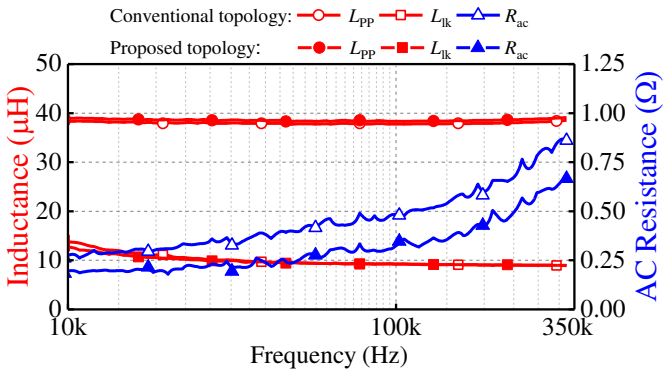

Fig. 11. AC resistance, R_{ac}, primary self-inductance, L_{PP}, and leakage inductance, L_{lk}, versus frequency for the proposed integrated transformer and inserted-segmental-shunt integrated transformer.

components of the LLC converter into only a single planar transformer while the converter operates properly.

REFERENCES

[1] K. Nathan, S. Ghosh, Y. Siwakoti, and T. Long, "A new DC–DC converter for photovoltaic systems: coupled-inductors combined Cuk-SEPIC converter," *IEEE Transactions on Energy Conversion,* vol. 34, no. 1, pp. 191-201, 2018.

[2] S. A. Ansari and J. S. Moghani, "A Novel High Voltage Gain Noncoupled Inductor SEPIC Converter," *IEEE Transactions on Industrial Electronics,* vol. 66, no. 9, pp. 7099-7108, 2018.

[3] A. Mirzaee, S. Arab Ansari, and J. Shokrollahi Moghani, "Single switch quadratic boost converter with continuous input current for high voltage applications," *International Journal of Circuit Theory and Applications,* vol. 48, no. 4, pp. 587-602, 2020.

[4] A. Mizani, S. A. Ansari, A. Shoulaie, J. N. Davidson, and M. P. Foster, "Single-active switch high-voltage gain DC–DC converter using a non-coupled inductor," *IET Power Electronics,* 2021.

[5] S. A. Ansari and J. S. Moghani, "Soft switching flyback inverter for photovoltaic AC module applications," *IET Renewable Power Generation,* vol. 13, no. 13, pp. 2347-2355, 2019.

[6] S. A. Ansari, J. N. Davidson, and M. P. Foster, "Evaluation of silicon MOSFETs and GaN HEMTs in soft-switched and hard-switched DC-DC boost converters for domestic PV applications," *IET Power Electronics,* 2021.

[7] S. Arab Ansari, J. S. Moghani, and M. Mohammadi, "Analysis and implementation of a new zero current switching flyback inverter," *International Journal of Circuit Theory and Applications,* vol. 47, no. 1, pp. 103-132, 2019.

[8] Y. Wei, Q. Luo, and A. Mantooth, "Overview of modulation strategies for LLC resonant converter," *IEEE Transactions on Power Electronics,* vol. 35, no. 10, pp. 10423-10443, 2020.

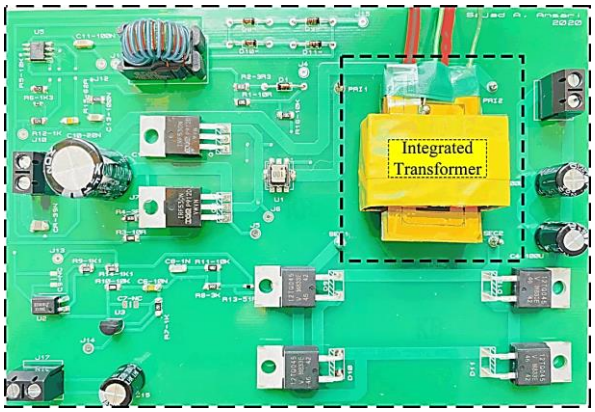

Fig. 12. Prototype of the designed LLC converter.

[9] Z. Fang, Z. Huang, H. Jing, and F. Liu, "Hybrid mode-hopping modulation for LLC resonant converter achieving high efficiency and linear behaviour," *IET Power Electronics,* vol. 13, no. 6, pp. 1153-1162, 2020.

[10] C. W. Tsang, M. P. Foster, D. A. Stone, and D. T. Gladwin, "Analysis and design of LLC resonant converters with capacitor–diode clamp current limiting," *IEEE Transactions on Power Electronics,* vol. 30, no. 3, pp. 1345-1355, 2014.

[11] S. A. Ansari, J. N. Davidson, M. P. Foster, and D. A. Stone, "Design and Analysis of a Fully-integrated Planar Transformer for LCLC Resonant Converters," in *2021 23rd European Conference on Power Electronics and Applications (EPE'21 ECCE Europe)*, 2021: IEEE, pp. P. 1-P. 8.

[12] S. De Simone, C. Adragna, and C. Spini, "Design guideline for magnetic integration in LLC resonant converters," in *2008 International Symposium on Power Electronics, Electrical Drives, Automation and Motion*, 2008: IEEE, pp. 950-957.

[13] Z. Ouyang, W. G. Hurley, and M. A. Andersen, "Improved Analysis and Modeling of Leakage Inductance for Planar Transformers," *IEEE Journal of Emerging and Selected Topics in Power Electronics,* vol. 7, no. 4, pp. 2225-2231, 2018.

[14] Z. Ouyang, J. Zhang, and W. G. Hurley, "Calculation of leakage inductance for high-frequency transformers," *IEEE Transactions on Power Electronics,* vol. 30, no. 10, pp. 5769-5775, 2014.

[15] Y. Zhang, D. Xu, K. Mino, and K. Sasagawa, "1MHz-1kW LLC resonant converter with integrated magnetics," in *APEC 07-Twenty-Second Annual IEEE Applied Power Electronics Conference and Exposition*, 2007: IEEE, pp. 955-961.

[16] J. Wang *et al.*, "Design of Integrated Magnetic Transformer for High Frequency LLC Converter," in *2020 4th International Conference on HVDC (HVDC)*, 2020: IEEE, pp. 986-991.

[17] S. Stegen and J. Lu, "Structure comparison of high-frequency planar power integrated magnetic circuits," *IEEE transactions on magnetics,* vol. 47, no. 10, pp. 4425-4428, 2011.

[18] A. Kats, G. Ivensky, and S. Ben-Yaakov, "Application of integrated magnetics in resonant converters," in *Proceedings of APEC 97-Applied Power Electronics Conference*, 1997, vol. 2: IEEE, pp. 925-930.

[19] Y. Liu, H. G. Wu, J. Zou, Y. Tai, and Z. Ge, "CLL Resonant Converter with Secondary Side Resonant Inductor and Integrated Magnetics," *IEEE Transactions on Power Electronics,* 2021.

[20] R. Muhammad, S. Kim, C. Suk, S. Choi, B. Yu, and S. Park, "Integrated Planar Transformer Design of 3-kW Auxiliary Power Module for Electric Vehicles," in *2020 IEEE Energy Conversion Congress and Exposition (ECCE)*, 2020: IEEE, pp. 1239-1243.

[21] W. Liu and J. Van Wyk, "Design of integrated LLCT module for LLC resonant converter," in *Twentieth Annual IEEE Applied Power Electronics Conference and Exposition, 2005. APEC 2005.*, 2005, vol. 1: IEEE, pp. 362-368.

[22] B. Li, Q. Li, and F. C. Lee, "High-frequency PCB winding transformer with integrated inductors for a bi-directional resonant converter," *IEEE Transactions on Power Electronics,* vol. 34, no. 7, pp. 6123-6135, 2018.

[23] M. D'Antonio, S. Chakraborty, and A. Khaligh, "Planar Transformer with Asymmetric Integrated Leakage Inductance Using Horizontal Air Gap," *IEEE Transactions on Power Electronics,* 2021.

[24] J. Zhang, Z. Ouyang, M. C. Duffy, M. A. Andersen, and W. G. Hurley, "Leakage inductance calculation for planar transformers with a magnetic

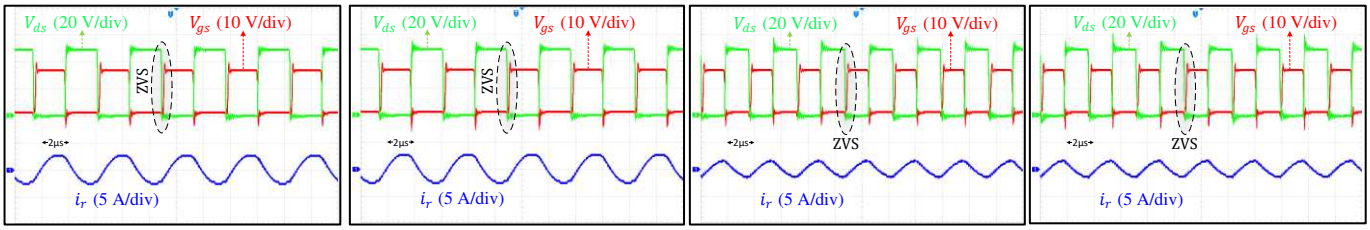

Fig. 13. Experimental waveforms of the designed LLC converter utilising (a) the proposed integrated transformer (f_s=210 kHz), (b) the inserted-segmental-shunt integrated transformer (f_s=210 kHz), (c) the proposed integrated transformer (f_s=280 kHz), (d) the inserted-segmental-shunt integrated transformer (f_s=280 kHz). V_{ds} is drain to source voltage, V_{gs} is gate to source voltage and i_r is the resonant current (defined in Fig. 1).

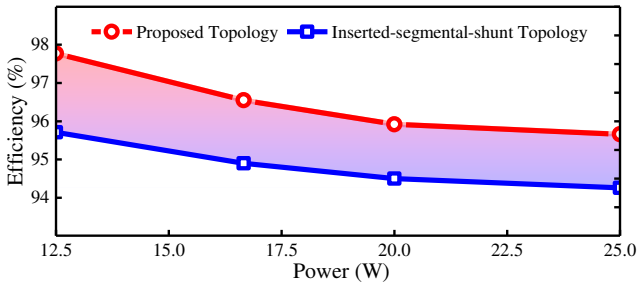

Fig. 14. Efficiency of the converter for the proposed topology and inserted-segmental-shunt integrated transformers.

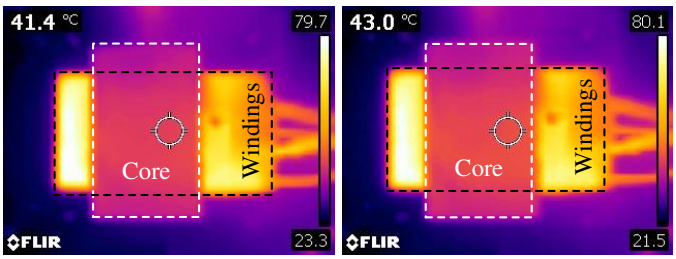

Fig. 15. Thermal images of the transformers. (a) Proposed topology. (b) Inserted-segmental-shunt topology.

shunt," *IEEE Transactions on Industry Applications,* vol. 50, no. 6, pp. 4107-4112, 2014.

[25] M. Li, Z. Ouyang, B. Zhao, and M. A. Andersen, "Analysis and modeling of integrated magnetics for LLC resonant converters," in *IECON 2017-43rd Annual Conference of the IEEE Industrial Electronics Society*, 2017: IEEE, pp. 834-839.

[26] M. Li, Z. Ouyang, and M. A. Andersen, "High-frequency LLC resonant converter with magnetic shunt integrated planar transformer," *IEEE Transactions on Power Electronics,* vol. 34, no. 3, pp. 2405-2415, 2018.

[27] S. A. Ansari, J. N. Davidson, and M. P. Foster, "Analysis, Design and Modelling of Two Fully-Integrated Transformers with Segmental Magnetic Shunt for LLC Resonant Converters," in *IECON 2020 The 46th Annual Conference of the IEEE Industrial Electronics Society*, 2020: IEEE, pp. 1273-1278.

[28] S. Arab Ansari, J. Davidson, and M. Foster, "Fully-integrated Planar Transformer with a Segmental Shunt for LLC Resonant Converters," *IEEE Transactions on Industrial Electronics,* 2021.

[29] S. A. Ansari, J. N. Davidson, and M. P. Foster, "Fully-Integrated Solid Shunt Planar Transformer for LLC Resonant Converters," *IEEE Open Journal of Power Electronics,* 2021.

[30] M. Noah, T. Shirakawa, K. Umetani, J. Imaoka, M. Yamamoto, and E. Hiraki, "Effects of secondary leakage inductance on the LLC resonant converter," *IEEE Transactions on Power Electronics,* vol. 35, no. 1, pp. 835-852, 2019.

[31] H.-S. Choi, "AN4151. Half-bridge LLC resonant converter design using Fairchild Power Switch (FPS)," *Fairchild semiconductor,* 2007.

[32] M. Noah, K. Umetani, M. Yamamoto, and J. Imaoka, "Winding orientation method to minimise the secondary leakage of a gapped transformer utilised in LLC resonant converter," *Electronics Letters,* vol. 54, no. 3, pp. 157-159, 2018.

[33] G. Spiazzi and S. Buso, "Effect of a split transformer leakage inductance in the LLC converter with integrated magnetics," in *2013 Brazilian Power Electronics Conference*, 2013: IEEE, pp. 135-140.

[34] H.-P. Park and J.-H. Jung, "Power stage and feedback loop design for LLC resonant converter in high-switching-frequency operation," *IEEE Transactions on Power Electronics,* vol. 32, no. 10, pp. 7770-7782, 2016.

[35] Y. Zhang, D. Xu, M. Chen, Y. Han, and Z. Du, "LLC resonant converter for 48 V to 0.9 V VRM," in *2004 IEEE 35th Annual Power Electronics Specialists Conference (IEEE Cat. No. 04CH37551)*, 2004, vol. 3: IEEE, pp. 1848-1854.

[36] W. G. Hurley and W. H. Wölfle, *Transformers and inductors for power electronics: theory, design and applications*. John Wiley & Sons, 2013.

[37] *Magnetics Ferrite Catalog*, Magnetics, 2013. [Online]. Available: www.mag-inc.com.

[38] S. De Simone, "LLC resonant half-bridge converter design guideline," *STMicroelectronics, Application Note AN2450,* p. 35, 2014.

Sajad A. Ansari was born in Shahrood, Iran, in 1994. He received the B.S. and M.S. degrees in electrical engineering from Shahrood University of Technology, Shahrood, Iran in 2016 and Amirkabir University of Technology, Tehran, Iran in 2019, respectively.

He is currently pursuing his PhD in the Department of Electronic and Electrical Engineering at The University of Sheffield, Sheffield, UK.

His research interests include renewable energy and design and control of power electronic converters.

Jonathan N. Davidson received the M.Eng. degree in electronic engineering and the Ph.D. degree in thermal modelling and management from the University of Sheffield, Sheffield, U.K., in 2010 and 2015, respectively.

In 2015, he became a Lecturer in electrical engineering at the University of Sheffield. He was made Senior Lecturer in 2022. His research interests include thermal modelling and management of power electronics, and the design and analysis of piezoelectric transformer-based power converters, high-voltage power supplies for plasma chemistry and waste-water sensing systems.

Martin P. Foster received the B.Eng. degree in electronic and electrical engineering, the M.Sc.(Eng.) degree in control systems, and the Ph.D. degree for his thesis "Analysis and Design of High-order Resonant Power Converters" all the University of Sheffield, Sheffield, U.K., in 1998, 2000, and 2003, respectively.

Since 2003, he has been a member of the academic staff in the Department of Electronic and Electrical Engineering, The University of Sheffield, where he is involved in power electronic systems. His current research interests include the modelling and control of switching power converters, resonant power supplies, multilevel converters, battery management, piezoelectric transformers, power electronic packaging, and autonomous aerospace vehicles.